PERFORMANCE OF SINGLE PHOTON-COUNTING X-RAY CHARGE COUPLED DEVICES

G. R. Riegler

R. A. Stern

K. Liewer

F. Vescelus

Jet Propulsion Laboratory

California Institute of Technology

Pasadena, CA 91109

J. A. Nousek and G. P. Garmire

Department of Astronomy

Pennsylvania State University

State College, Pennsylvania

PERFORMANCE OF SINGLE PHOTON-COUNTING X-RAY CHARGE COUPLED DEVICES

G. R. Riegler, R. A. Stern, K. Liewer, and F. Vescelus
Jet Propulsion Laboratory, California Institute of Technology
Pasadena, CA 91109

and

J. A. Nousek and G. P. Garmire
Department of Astronomy, Pennsylvania State University
State College, Pennsylvania

ABSTRACT

Results of initial performance tests on x-ray sensing properties of charge-coupled devices (CCDs) are presented. CCDs have demonstrated excellent spatial resolution and good spectral resolution, superior to that of non-imaging proportional counters.

I. INTRODUCTION

A charged coupled device (CCD) can be expected to combine the best properties of high-resolution imaging detectors and solid-state spectrometers, namely high spatial resolution and moderate spectral resolution, at high efficiency. Because of the importance of such a device for x-ray astronomy, a number of researchers have begun laboratory studies of x-ray CCDs (Griffiths et. al. 1981 and reference therein). This paper describes the status of x-ray CCD studies at the Jet Propulsion Laboratory.

Elsewhere within this conference, reviews of the known properties and open questions for a wide range of galactic and extra-galactic sources have been presented. These reviews have called for moderate resolution, e.g., $E/\Delta E \sim 40$ at $E \sim 6$ keV, which CCDs are expected to provide. The ability to produce a spectrum for each image element (pixel) is important for the studies of supernova remnants, clusters of galaxies, and wherever source confusion would be a problem for non-imaging solid state spectrometers.

II. DESCRIPTION OF THE TEST CAMERA

Several CCD cameras have been built at JPL for the study of CCDs and for the testing of CCDs to be used by the Galileo Jupiter orbiter and the Wide Field Planetary Camera of the Space Telescope. Two cameras were used in these tests, one for the virtual phase devices (Janesick et al., 1981) and the other for the three phase devices (Blauke et al., 1981). The timing and amplitude of the clock pulses required to shift the data out of the two types of CCDs differ, but all the amplifiers and signal processing circuits are identical.

The signal processing circuitry uses a double correlated sampler where output is digitized to 16 bits. The pixels are clocked out at a rate of 5×10^4 pixels per second which minimizes the noise associated with sampler. These items plus very careful camera layout allow us to achieve a noise figure of 4.5 electrons RMS for the camera system and an amplifier noise of 7 electrons for the virtual phase CCD or 13 electrons for the three phase CCD. The difference in read noise is due to differences in the on chip amplifiers.

The CCDs are contained in a vacuum chamber which is evacuated to a pressure of a few Torr. Cooling is accomplished by a regulated flow of liquid nitrogen. The temperature can be varied from room temp to -190°C with a stability of 0.1°C. A shutter in the vacuum chamber controls the exposure for all the sources used.

The removable front face of the vacuum chamber can hold an optical window, a beryllium foil window, or the window can be replaced by a flourescent X-ray source with interchangeable targets which is activated by a 1mCu source of alpha particles.

The CCDs used in these tests were all manufactured by Texas Instruments Co. Both the three phase and virtual phase devices have 15.2 micron square pixels in 800 x 800 arrays. The three phase devices were thinned to approximately 10μ and operated with the radiation incident from the non-circuit side (backside). The virtual phase CCD is a thick device and the radiation is incident on the circuit side. Because the virtual phase CCDs have only a single gate structure, the circuit layer is thin (0.6 micron). There is an additional 0.5 micron protective overcoat. While the absorbtion in these layers would require that the CCD be thinned and run in the back illuminated mode for energies below one kilovolt, thinning was not required for these tests (80% transmission at 1.5 keV).

Although the virtual phase device is 250 microns thick it is a layered structure with only a 10 micron thick layer adjacent to the gate structure that acts as an active detector region for x-rays.

For the tests described here the CCDs were cooled to about -100°C. At this temperature the dark current is near $10^{-2}e^-$/pixel/sec for the 3-phase device and $10^{-3}e^-$/pixel/sec for the virtual phase. Our exposure times vary from 1 to 30 seconds depending on which source is used and so dark current is completely negligible. The virtual phase devices have an additional noise source which comes from currents generated within the device when it is clocked. This noise source amounted to 40 electrons RMS for the device used in these tests.

A more complete description of the 3-phase device was given by Blauke et al. (1981). The virtual phase device was described by Janesick et al. (1981).

III. X-RAY PERFORMANCE

Both three-phase and virtual-phase CCDs were illuminated with 5.9 keV x-rays from a Fe 55 source. Figure 1 shows a portion of a pseudo-image which displays relative amount of charge for each pixel. With the array orientation shown in Figure 1, events are transferred out (charge-coupled) in a downward direction in each column. Some "smearing" along the vertical direction is apparently due to incomplete charge transfer and is frequently referred to as "deferred charge". The gray scale of the image is highly "stretched" to reveal this low-level incomplete charge transfer.

The distribution of individual pixel event sizes is shown in Figure 2. The "background" curve is off scale below relative event size 7200. The response to Fe 55 x-rays is shown by the peak near event size 7720.

To account for charge smearing along the read-out direction and the finite probability of charge deposition in two adjacent pixels, various data summation techniques have been used. Figure 3 shows the histogram of the number of events as a function of relative event size for pixels when the deferred charge is included with the main event charge. Starting with the main event, the computer algorithm for this approach adds the charge for successive pixels in a vertical column below the initial event until the pixel charge is less than two standard deviations above an average background level. Figure 4 shows the same set of data as in Figure 3, except that those events have been excluded for which the main charge deposition was observed in two adjacent pixels. It is apparent that, compared to the histogram in Figure 3, the background events below the energy peak have been significantly reduced.

Figure 4 represents the best performance obtained so far in an x-ray CCD. The full width at half maximum response (FWHM) is ~ 12%, corresponding to an energy resolution of 700 eV FWHM. In order to obtain the equivalent RMS noise figure, which is frequently used to characterize CCDs, we use a conversion factor of 8.5 (3.6 eV/electron-hole pair x 2.35, the number of standard deviations per FWHM). The noise performance in Figure 4 corresponds to 74 electrons equivalent RMS noise. Figure 5 was derived from the same set of data as in Figure 2 through 4 except that a 3 x 3 mask was used for the array of pixels to be included for each event. A somewhat better performance is obtained in Figure 6 where a rectangular mask of 2 x 6 pixels was used; the mask was aligned along the charge readout direction. In the latter two cases, no additional correction for incomplete charge transfer was made.

The performance for virtual-phase CCDs is comparable to that of 3-phase CCDs except that a poorer noise performance was obtained. From tests at optical wave lengths it was observed that additional charge is created in the serial register under the clocked well. This amount of charge, which appears to be a function of the clock pulse shape, contributed to poor noise performance at optical and x-ray wavelengths. Figure 7 shows the response of a virtual-phase CCD to Fe 55 x-rays. Comparable graphs for sulfur x-rays (2.3 keV) and aluminum x-rays (1.49 keV) are shown in Figures 8 and 9.

IV. PRESENT AND EXPECTED PERFORMANCE

The best noise performance achieved to date with visible light was 8.8 electrons rms for a three-phase device and 22 electrons rms for a virtual-phase CCD. The average widths observed in visible-light tests are 22 electrons and 44 electrons, respectively. Compared to these values, the results for mono-energetic x-rays of 5.9 keV are still significantly poorer.

The most recent analysis of x-ray calibrations shows that the depth of the active regions deduced from optical tests is in fact consistent with the detection efficiency as determined from x-ray absorption measurements and the manufacturer's specifications, i.e., 10 microns.

Spatial resolution obtained is comparable to the size of a pixel, i.e., 15 microns x 15 microns. This pixel size corresponds to an angular resolution of 1/3 arc second for a telescope of 10 meter focal length, for example, for an AXAF.

V. SUMMARY

The preceding data show conclusively that CCDs have excellent spatial resolution and good spectral resolution, superior to non-imaging proportional counter resolution. However, further research is required to understand the difference between the noise performance at optical and x-ray wavelengths. Various techniques to optimize CCD performance for x-ray applications need to be explored, but these preliminary results are clear evidence that CCDs will become an important tool for x-ray astronomy.

REFERENCES

Blauke, M., Janesick, J., Hall, J., and Cowens, M. 1981, Proc. S.P.I.E., 290.

Griffiths, R. E., Polucci, G., Mak, A., Murray, S. S., and Schwartz, D. A. 1981, Proc. S.P.I.E., 290 (in press).

Janesick, J., Hynecek, J., Blouke, M. 1981, Proc. S.P.I.E., 290.

ORIGINAL PAGE
BLACK AND WHITE PHOTOGRAPH

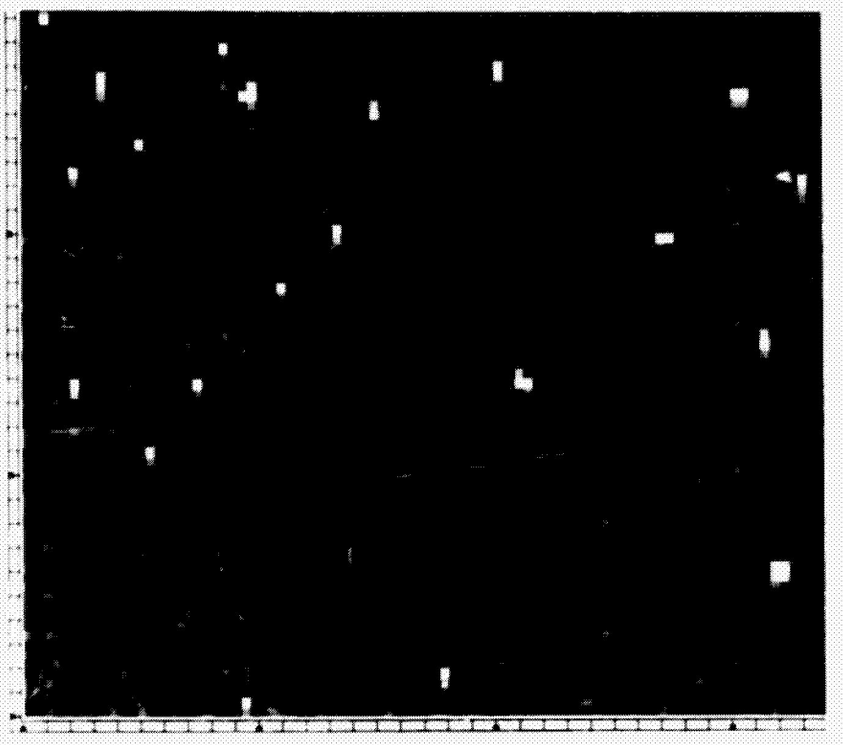

FIGURE 1

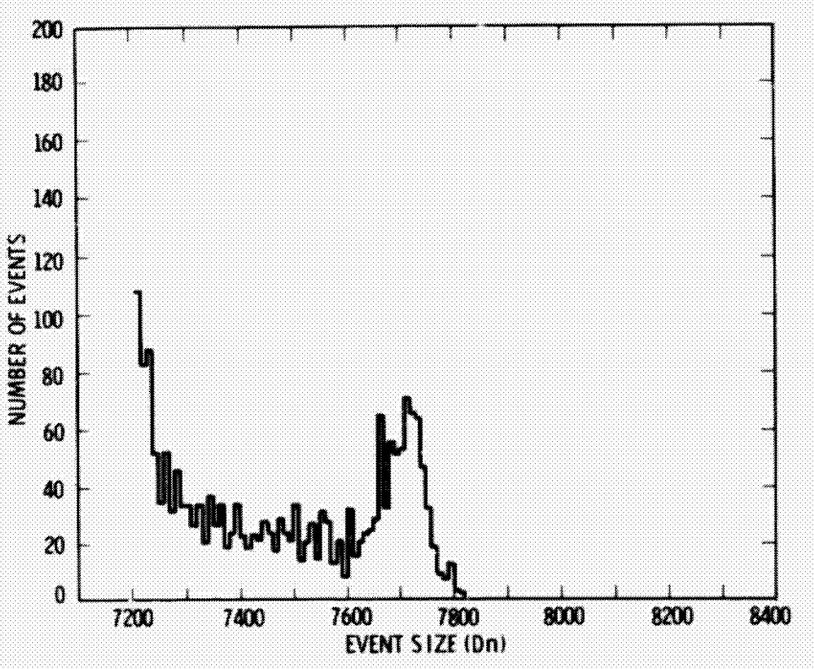

FIGURE 2

3-PHASE CCD: Fe55, ADJACENT EVENTS INCLUDED

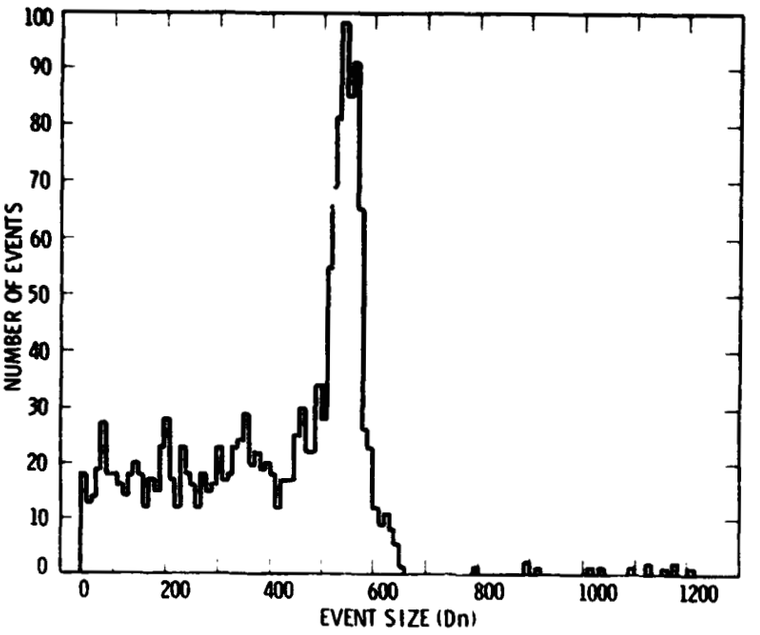

FIGURE 3

3-PHASE CCD: Fe55, ADJACENT EVENTS EXCLUDED

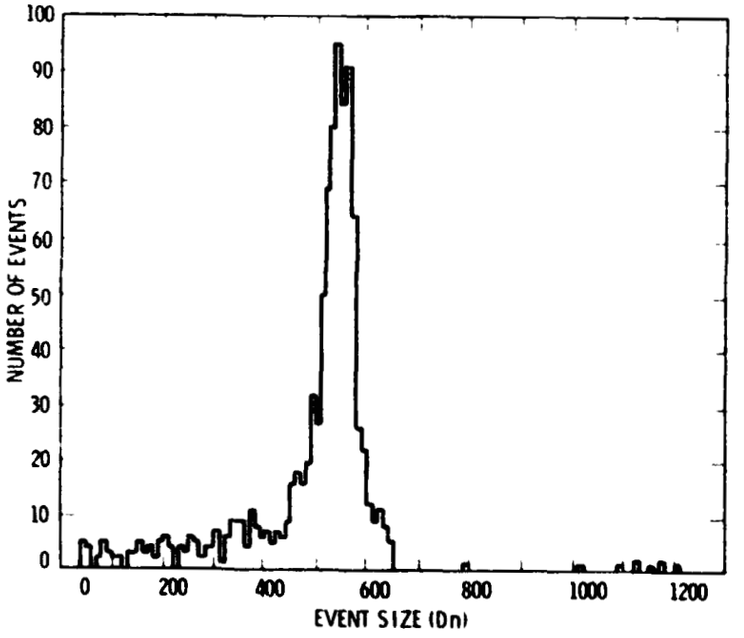

FIGURE 4

3-PHASE CCD: Fe55, 3 × 3 MASK

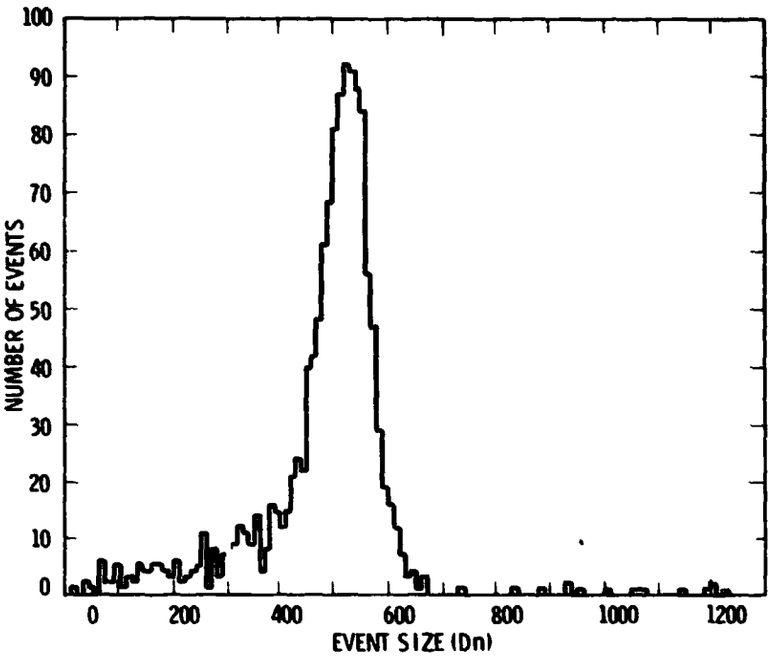

FIGURE 5

3-PHASE CCD: Fe55, 2 × 6 MASK

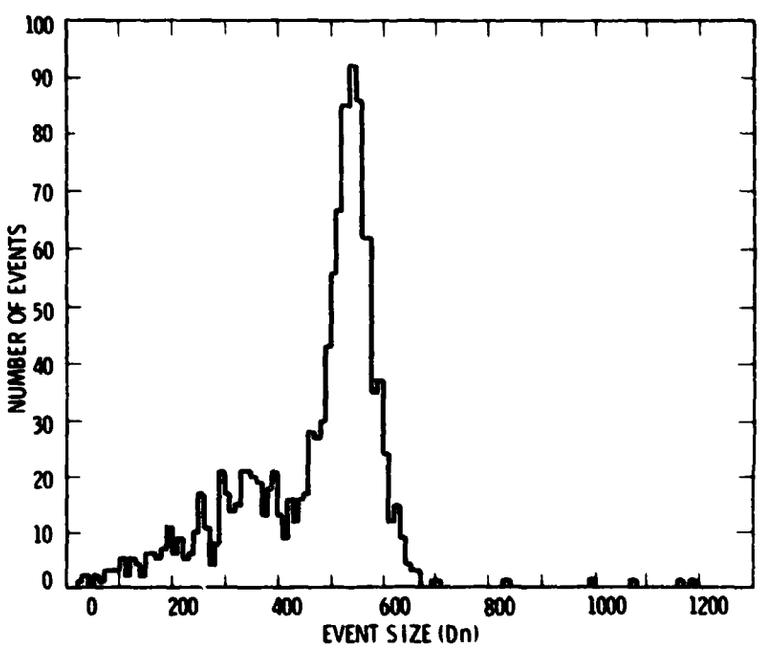

FIGURE 6

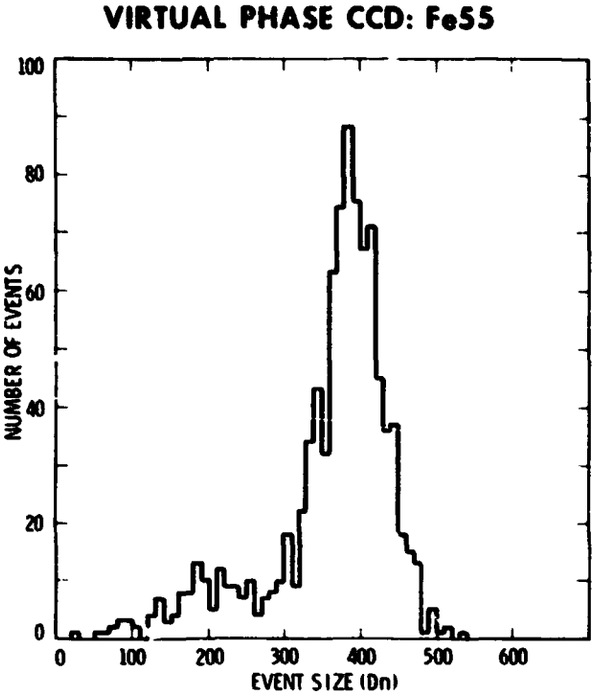

FIGURE 7

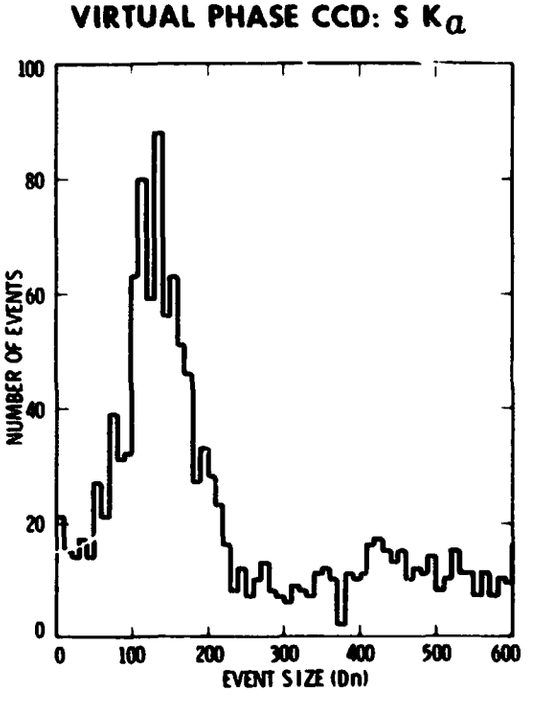

FIGURE 8

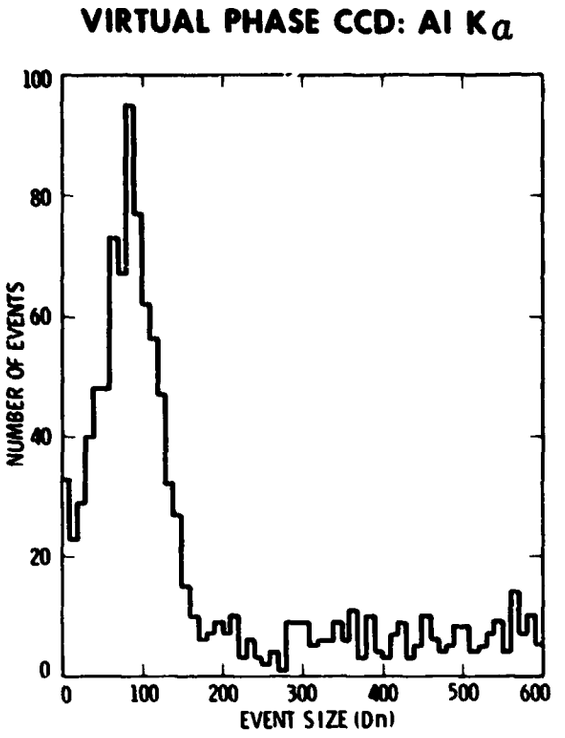

FIGURE 9